NF

NASA Technical Memorandum 83247

(NASA-TM-83247) ANALYSIS OF UV PROTECTION REQUIREMENTS AND TESTING OF CANDIDATE ATTENUATORS FOR THE HALOE OPTICAL INSTRUMENT (NASA) 29 p HC A03/MF A01 CSCL 14B

N82-18652

Unclas
G3/42 09011

ANALYSIS OF UV PROTECTION REQUIREMENTS AND TESTING OF CANDIDATE ATTENUATORS FOR THE HALOE OPTICAL INSTRUMENT

JOHN E. NEALY, WILLIAM K. GOAD, AND
D. MICHELE HEATH

DECEMBER 1981

National Aeronautics and
Space Administration

Langley Research Center
Hampton, Virginia 23665

SUMMARY

Results of calculations are presented which simulate photolytic processes occurring in HALOE gas calibration cells exposed to extra-terrestrial solar ultraviolet photons. These calculations indicate that significant photolysis takes place in two of the sapphire-enclosed cells over the exposure periods of the proposed mission. A subsequent laboratory investigation is also described in which a high-voltage discharge hydrogen light source is used in conjunction with a vacuum ultraviolet spectrograph. The UV emission from this lamp was used to expose two candidate UV attenuators (ZnSe and coated Ge) to ascertain their suitability as UV filters while maintaining original infrared optical properties. Both materials were found to be effectively opaque to vacuum UV radiation and suffered no adverse effects regarding their infrared transmissivity.

INTRODUCTION

The HALOE (Halogen Occultation Experiment) project was conceived as a means of measuring and monitoring trace species in the upper atmosphere of importance to chemical processes occurring there. The measurements are to be made from a satellite platform utilizing techniques of infrared gas-filter spectroscopy. Details regarding the measurement strategy and methodology are described in reference 1. The optical instrument which has been designed for making the measurements incorporates a system that permits periodic precision calibration of the detectors to be made during the mission. The calibrations are performed by insertion of four sealed cells into the unattenuated solar beam. The calibration cells contain known amounts of the same gases which are to be measured in the stratosphere (NO, HCl, HF, CH_4). The window material for the cells is sapphire, chosen for its excellent infrared transmittance. However, sapphire also transmits radiation well into the vacuum ultraviolet region, and the gaseous contents of the cell may be subject to photodissociation. Photochemical calculations have been made using a modified atmospheric chemistry model. The results of the calculations indicate that the cells containing NO and HCl will undergo significant photolysis over the proposed 2-year mission.

It was concluded from these calculations that experimental verification and testing of a suitable filter material would be highly desirable. A laboratory setup consisting basically of a UV light source, a vacuum spectrograph, and calibrated photodetector was assembled. At first, a series of stability tests at desired operating conditions and measurements of spectral characteristics of the lamp were performed. After these lamp properties were established, testing of candidate filter materials (zinc selenide and germanium) commenced, in which the samples were irradiated with known exposures of UV light. Infrared transmittance characteristics of the samples were measured before and after testing. The following sections discuss the calculations, some operational details of the experimental procedures, and results of the filter tests.

CALCULATIONS OF CALIBRATION CELL PHOTOLYSIS

The calibration cells are sealed cylindrical containers, 4 cm in length and 2.5 cm in diameter having sapphire windows of 1-mm thickness. Each cell contains a mixture of the active gas and nitrogen as an inert filler. The table below indicates the nominal total pressures and mole fractions of the constituents for the cells used in the following analysis:

Gas	Total Pressure, Atm.	Mole Fraction of Active Gas
NO	0.04	0.01
HCl	0.04	0.02
CH_4	0.30	0.60
HF	0.03	0.003

Figure 1 shows a diagram of the HALOE optical instrument, and the physical position of the calibration cells in the optical train is indicated. For the proposed satellite mission, the cells are to be inserted into the incoming solar beam for a 7.12-second time period, allowing calibration of the instrument. This procedure is repeated for each cell at 45-minute intervals throughout the entire 2-year period of the mission. This translates into a net exposure for each cell of about 2 days.

All of these gases photolyze to some degree when exposed to ultraviolet photons, and the extent of this photolysis is dependent on wavelength and intensity. The cross sections for photolysis of the gases under consideration and the transmittance of sapphire in the wavelength region of interest are shown in figure 2. The sapphire transmittance is taken from a manufacturer's nominal specification chart for UV grade material. It is immediately apparent that UV radiation will be transmitted in the spectral region where NO and HCl undergo photodissociation. For CH_4, the photo-absorption cross section is decreasing rapidly with wavelength where sapphire is beginning to transmit, and resultant dissociation is expected to be less than that for NO and HCl. The cross section data and corresponding photolysis rate are those used in the atmospheric chemistry model of reference 2. Apparently, very little quantitative data are available for properties of HF in the vacuum UV region; however, the qualitative absorption of HF as presented in reference 3 indicates that any UV absorption by this species occurs at wavelengths much shorter than the cutoff wavelength for sapphire as is shown in figure 2. Consequently, study of photolytic destruction of HF was not included in the present investigation.

Cross section and solar flux data in existing atmospheric chemistry models predict that dissociation of NO will be most severe, with HCl and CH_4 being respectively less. Hence, more emphasis was placed on analyzing the behavior of the NO cell. During the last decade, several investigators have studied photodissociation of NO. Reference 4 is particularly comprehensive, and

concludes that most photolysis results from absorption in the δ(0-0) and δ(1-0) transitions. The rate for photodestruction due to these transitions is given in reference 4 as 1.3×10^{-5} sec^{-1}. This value has been reevaluated in reference 5 on the basis of more recent solar fluxes and oscillator strengths as 3.7×10^{-6} sec^{-1}.

In anticipation of more refined computations and laboratory investigations, a computer algorithm was developed to calculate the line-by-line absorption coefficient for the NO δ-bands. Using spectroscopic constants from references 4 and 5, the detailed spectral absorption from these two bands has been calculated and plotted results are given in figure 3. Each line on the plot represents the value of peak absorption determined from the formulas of reference 6. The calculations were performed for nominal room temperature conditions of 300 K at the cell pressure of 0.04 atm., for which it was found that Doppler broadening dominated the line shape. The Doppler half-width was determined to be 0.122 cm^{-1}, about 36 times as great as the estimated collision width. An approximate photodissociation rate, J , may be calculated from

$$J \simeq \frac{\overline{F_{\Delta\nu}}}{\Delta\nu} \int_{\Delta\nu} \phi_\nu \sigma_\nu d\nu$$

where $\Delta\nu$ is the wave number range for the band, σ_ν is the spectral cross section, and F_ν is the UV flux. The quantum efficiency for photolysis, ϕ_ν , is here assumed to be unity, in accordance with previous model calculations. The integrated absorption, $\int_{\Delta\nu} \sigma_\nu d\nu$, for the δ(0-0) and δ(1-0) bands is computed to be 1.926×10^{-15} and 4.728×10^{-15} cm, respectively. When nominal solar flux in this wavelength region is assumed (2.8×10^{11} photons/cm^2) and a bandpass of 600 cm^{-1} is used for each band, the resultant photolysis rates are 0.9×10^{-6} and 2.2×10^{-6} sec^{-1} for the δ(0-0) and δ(1-0) bands, respectively. These results are in substantial agreement with those of reference 5.

The primary photolytic breakup of NO and HCl molecules into constituent atoms initiates a series of chemical reactions which inevitably result in a buildup of stable species at the expense of the parent gas. In order to predict realistically the sequence of events taking place in the cells on exposure to UV radiation, pertinent sections of a photochemical model were employed (ref. 1). The reaction schemes for NO and HCl are given in Table I. For methane, the photolysis rate was determined to be 6.5×10^{-10} sec^{-1} for wavelengths in the sapphire transmission region. This small value precludes any significant dissociation of CH_4, and this species was not given further consideration. The exposure cycle consists of a short period of illumination during which photolytic reactions occur, and a much longer dark period in which only thermochemical reactions take place. The calculations for each individual cycle differ because the initial conditions for each illumination period continue to vary. The history of the variation of dominant species during the first exposure cycle is shown in figure 4. It is seen that N and O atoms equilibrate during the first millisecond. Molecular nitrogen, oxygen, NO_2,

and N_2O form continuously during the exposure time. When the radiation is shut off, O and N disappear rapidly while N_2, O_2, NO_2, and N_2O remain essentially unchanged by reactions occurring in the dark portion of the cycle. Thus, steadily increasing amounts of stable species form as NO is destroyed. The intermediate species included in the reaction scheme (O_3, $O(^1D)$, NO_3, N_2O_5) form in small quantities during the illumination period and subsequently disappear during the dark period.

The total time of the mission includes over 23,000 such cycles. After calculating in detail about 10,000 cycles, the irreversible disappearance of NO became obvious. Figure 5 depicts the predicted disappearance of NO for the complete mission. (The latter half of the curve is based on an exponential function extrapolation.)

Similar types of calculations for the HCl cell showed that substantial amounts of HCl would also be irreversibly destroyed. This was not unexpected since the photolysis rate was determined to be 2.5×10^{-6} sec^{-1}, only slightly less than that determined for NO.

The calculations described above were also used to estimate the UV attenuation required such that no more than 5% of the parent gas be depleted. Using appropriate solar flux values for the pertinent wavelength ranges, the attenuation factors were found to be 98.6% and 93.9% for NO and HCl, respectively, or a 1.4% and 6.1% transmission of incident solar flux would be the maximum allowable. Calculations of this sort are necessarily idealizations of the actual situation, since many of the rate coefficients and cross sections are imprecisely known. Also, the possibility exists that important but unknown chemical mechanisms may not have been included. In order to test in a positive manner that the UV intensity is sufficiently attenuated, and that the attenuators suffer no deleterious effects from sustained UV exposure which might impact the mission measurements, laboratory verification is highly desirable.

TEST INSTRUMENTATION AND PROCEDURE

A UV light source which had been previously utilized in an experiment related to high-speed planetary entry was employed in the present tests. The illumination, which is provided by a high voltage discharge in hydrogen, was felt to be of sufficient intensity in the desired spectral region for testing candidate attenuators. Characteristics of this light source have been described in detail in reference 8. Figure 6 shows a typical photon flux spectrum for the lamp when used in conjunction with a 1-meter vacuum spectrograph. Also shown is the solar flux outside the atmosphere taken from the photochemical model of reference 2. It is seen that at about 170 nm, the lamp and solar flux are approximately equal. The lamp flux can be increased to about 10 times the level shown in figure 6 by increasing entrance and exit slit widths (at some sacrifice in spectral resolution). It is thus apparent that meaningful testing of the cells and/or candidate UV attenuators may be carried out conveniently. For this study, attenuators made of zinc selenide and germanium have been selected.

The instrumentation used in the experiment is depicted in figure 7. A 1-meter scanning monochromator was used in conjunction with the hydrogen discharge UV light source. A high vacuum (< 2 x 10^{-5} mm Hg) was maintained in the main chamber of the spectrograph during operation of the lamp. Parameters such as hydrogen flow rate, pressure, current, and voltage on the lamp were closely monitored and held constant throughout the experiment. The exit aperture of the spectrograph was equipped with a dual-beam attachment containing grazing incidence mirrors to deflect the beam into one of two available testing chambers. Light detectors used were either a high-gain photomultiplier tube placed behind a sodium-salicylate coated window, or a photodiode detector recently calibrated at NBS. Options for readout of the detector signals included a strip chart recorder, a dc voltmeter, and an integrating digital voltmeter.

The assembly is represented schematically in figure 8. Pressure and flow rate of hydrogen from a supply bottle to the lamp were regulated through a series of valves and gages. Both the gas flowmeter and the pressure gage readouts were augmented by digital voltmeters for more precise regulation. A constant current power supply was used to maintain a 160 ma current on the lamp. The light source was cooled by both water and air flow systems.

A magnesium fluoride window separating the lamp from the spectrograph main chamber was found to be unsuitable for this experiment. A continuous drop in transmittance was observed after several hours of lamp operation, and visual examination of the exposed window indicated significant degradation. This necessitated operation of the system without a window and required compensating adjustments of the lamp pressure and flow rate. Pressure in the main chamber was raised but remained sufficiently low (< 2 x 10^{-5} mm Hg) to prevent attenuation and optical surface deterioration.

Prior to testing the attenuators, the lamp was operated and close observation was made of the system's behavior. Figure 9 shows a scan of the lamp's hydrogen spectrum from 140 to 165 nm, along with the quantum efficiency of the photodiode detector as determined by NBS. The quantum efficiency is seen to be nearly constant in this wavelength interval. The intensity of the hydrogen spectrum exhibits the features of a continuum between 165 and 200 nm as is shown in figure 10, where the detector gain is larger than for the scan of figure 9. The signal from the photodiode for several wavelengths in this continuum region was measured by integrating the voltage over a time period of 100 seconds and averaging, thus eliminating minor short-term fluctuations. This procedure was repeated several times over a period of about a week. Results from these observations are shown in figure 11 and indicate that under controlled conditions, the lamp exhibited very good repeatability and spectral stability.

MEASUREMENT STRATEGY AND TEST RESULTS

Two infrared transmitting materials were selected as candidate UV attenuators for the present tests. These were samples of uncoated zinc selenide and pure germanium with an antireflective coating. The measurement requirements included

irradiation of the sample with UV photons such that the exposure is representative of that incurred during the orbital mission. In order to accomplish this, the total lamp radiance is focused by the grating on the exit aperture. The dimensions of the spectrograph entrance slit were fixed at 50 μm width and 5 mm height. The rectangular concave grating is equidistant from both entrance and exit slits, with geometry such that the angles of divergence of radiation from the focused image of the entrance slit are 5.55° in the horizontal and 3.25° in the vertical.

A two-position grazing incidence concave mirror is situated in the dual-beam chamber so that the exit image is directed in either of two directions, as is illustrated in figure 12. For the test configuration, the sample attenuators were placed so that the exposed surface was 5 mm from the focused slit image. This rendered an illuminated area of 0.5 x 5.28 mm, or 0.0264 cm^2, on the surface of the test samples. Prior to exposing the samples to UV photons, infrared transmission scans for each sample were generated by utilizing facilities provided by the LaRC Instrument Research Division.

The samples were then irradiated for a specified 48-hour time period, after which the infrared transmittance measurements were repeated in order to ascertain whether the infrared properties of the materials had been altered. To operate the UV light source for more than about 3 hours continuously was deemed inadvisable, and the 48-hour total exposures were normally performed over an interval of a week or more. The operational configuration was established so that the test sample was positioned in one path of the dual-beam chamber, and the calibrated photodiode in the other. The initial warm-up period for the light source was about 30 minutes, during which time the samples were not exposed to light. After the lamp intensity had stabilized with time, as monitored by the photodiode signal, the samples were then exposed for a period of several hours. During these exposure sessions, the photocurrent of the calibrated diode was recorded periodically (at least hourly) by momentarily deflecting the beam onto the diode and reading the photocurrent with an electrometer. The stability and repeatability tests performed earlier provided confidence that more frequent observations were unnecessary.

The calibrated photodiode signal currents recorded during the sample exposures are shown in figure 13 as a function of total exposure time. In addition, an ordinate scale representing photon flux is provided. Since the photodiode signal current is a direct measure of the number of electrons emitted by the photocathode of the detector, the incidence number of photons may be determined from the previously measured quantum efficiency of the detector. When it is assumed that the quantum efficiency is constant (as it practically is for the wavelength region where most of the lamp emission occurs), the number of photons per second incidence on the photodiode is given by

$$N(\text{photons/sec}) \approx \frac{6.24(10)^{18} i_D}{\eta}$$

where i_D is the signal current in amperes and η is the quantum efficiency, which has been assigned the value 0.065 (see figure 3).

The photon flux incident on the sample is then found by dividing by the area illuminated. By referring to figure 6, it may be seen that this flux is on the order of 100 times the unattenuated solar flux in the wavelength region where nitric oxide absorbs, and exceeds the solar flux to an even greater degree at shorter wavelengths.

The infrared transmission measurements are shown in figures 14 and 15 for the ZnSe and Ge samples, respectively, for times before and after UV exposures. No apparent differences are immediately discernible; indeed, after careful scrutiny of the transmission measurements made with several infrared spectrometers, it was concluded that no measurable alteration of the infrared properties of either of the samples occurred as a result of the UV irradiation.

In addition to the exposure measurements, attempts were made to observe any UV radiation transmitted through the samples. This was accomplished by observing signals from a high-gain photomultiplier tube/sodium salicylate window combination placed directly behind the sample in the dual-beam chamber. With the sample in place, only dark current could be detected, which guaranteed the UV attenuation factor to be at least 10^{-4}. This degree of attenuation greatly exceeds that required for insuring that the calibration cells are safe from photolytic degradation.

CONCLUSIONS

There are two primary conclusions resulting from this investigation:

1. Calibration gas cells enclosed in sapphire containing nitric oxide or hydrochloric acid gas are subject to substantial photolytic effects when irradiated with unattenuated solar UV photons.

2. The infrared transmitting materials, ZnSe and Ge, are suitable as UV attenuators and should suffer no adverse effects when exposed to photon fluxes up to 100 times the unattenuated solar flux in the vacuum ultraviolet spectral region.

Since the antireflective coated germanium sample exhibits infrared transmissivity greater than 90% over the crucial wavelength range (2.5-10 μm), while that of ZnSe is slightly less than 75%, the former material appears to be more suitable. Particular apprehension about the optical coating was felt; however, no deleterious effects whatsoever could be detected as a result of the UV exposure.

The utilization of instrumentation and techniques as described herein may be feasible in fundamental studies related to photodissociation of trace gases in the earth's atmosphere. For example, several species important in the chemistry of the upper atmosphere have reasonably well-known absorption

cross sections in the vacuum UV, while the quantum efficiencies for photolysis are not known as a function of wavelength. The subject source along with its peripheral equipment may be well-suited as a tool for measuring spectral quantum efficiencies.

REFERENCES

1. Russell, J. M.; Park, J. H.; and Drayson, S. R.: "Global Monitoring of Stratospheric Halogen Compounds from Satellite Using Gas Filter Spectroscopy in the Solar Occultation Mode." Appl. Opt., Vol. 16, No. 3, March 1977, pp. 607-612.

2. Boughner, R. E. and Nealy, J. E.: "A Coupled Radiative-Convective-Photochemical Model of the Stratosphere." NASA TP-1148, April 1979.

3. Waggoner, M. G.; Chow, K. W.; and Smith, A. L.: "Direct-Reading Absorption Spectrometer in the Windowless Vacuum-Ultraviolet: Absorption Spectra of He_2, HF, and N_2." Chem. Phys. Lett., Vol. 3, No. 3, March 1969, pp. 151-154.

4. Cieslik, S. and Nicolet, M.: "The Aeronomic Dissociation of Nitric Oxide." Planet. Space Sci., Vol. 21, 1973, pp. 925-938.

5. Frederick, J. E. and Hudson, R. D.: "Predissociation of Nitric Oxide in the Mesosphere and Stratosphere." J. Atmos. Sci., Vol. 36, 1979, pp. 737-745.

6. Whiting, E. E.: "An Empirical Approximation to the Voigt Profile." J. Quantum Spectroscopy Radiation Transfer, Vol. 8, 1968, pp. 1379-1384.

7. Natarajan, M.: "Model Studies of the Natural and Perturbed Stratosphere." Ph. D. Thesis, State University of New York, 1976.

8. Nealy, J. E.: "Absolute Calibration of a Hydrogen Discharge Lamp in the Vacuum Ultraviolet." NASA TM X-3327, December 1975.

TABLE I

(a) Chemical Reaction Mechanisms Used for NO Cell Calculations

$NO + h\nu = N + O$	$2O + M = O_2 + m$	$O^* + N_2 = O + N_2$
$O_3 + h\nu = O + O_2$	$O + O_2 + M = O_3 + M$	$O + O_3 = 2O_2$
$^{\dagger}O_3 + h\nu = O^* + O_2$	$O_3 + NO = NO_2 + O_2$	$NO + O + M = NO_2 + M$
$NO_2 + h\nu = NO + O$	$O_3 + NO_2 = NO_3 + O_2$	$O^* + N_2 + M = N_2O + M$
$NO_2 + h\nu = O^* + NO$	$NO + NO_3 = 2NO_2$	$N_2O + O^* = N_2 + O_2$
$NO_3 + h\nu = NO + O_2$	$NO_2 + O + M = NO_3 + M$	$N_2O + O^* = 2NO$
$NO_3 + h\nu = NO_2 + O$	$NO_2 + NO_3 + M = N_2O_5 + M$	$N_2O_5 + O = 2NO_2 + O_2$
$N_2O + h\nu = N_2 + O^*$	$N_2O_5 + M = NO_2 + NO_3 + M$	$N + NO_2 = N_2O + O$
$N_2O_5 + h\nu = NO_2 + NO_3$	$N + O_2 = NO + O$	$N + NO = N_2 + O$
$O_2 + h\nu = 2O$	$N + O_3 = NO + O_2$	$O + NO_2 = NO + O_2$
$2N + M = N_2 + M$	$O^* + O_2 = O + O_2$	

(b) Chemical Reaction Mechanisms Used for HCl Cell Calculations

$HCl + H\nu = H + Cl$

$Cl_2 + h\nu = 2Cl$

$H + HCl = H_2 + Cl$

$Cl + H_2 = HCl + H$

$2Cl + M = Cl_2 + M$

$2H + M = H_2 + M$

$H + Cl + M = HCl + M$

$H + Cl_2 = HCl + Cl$

†The original O* is used for the excited ^1D state of the oxygen atom

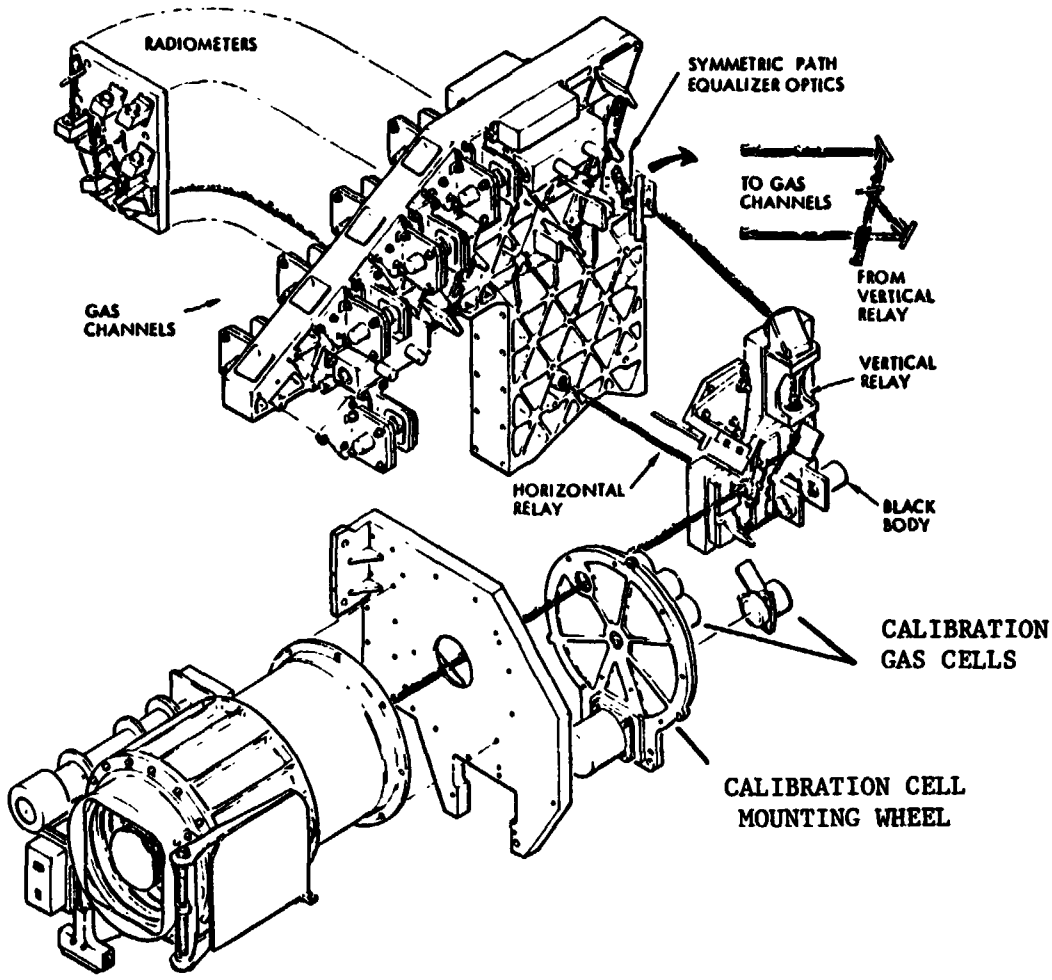

Figure 1.-HALOE optical instrument assembly diagram showing position of calibration gas cells.

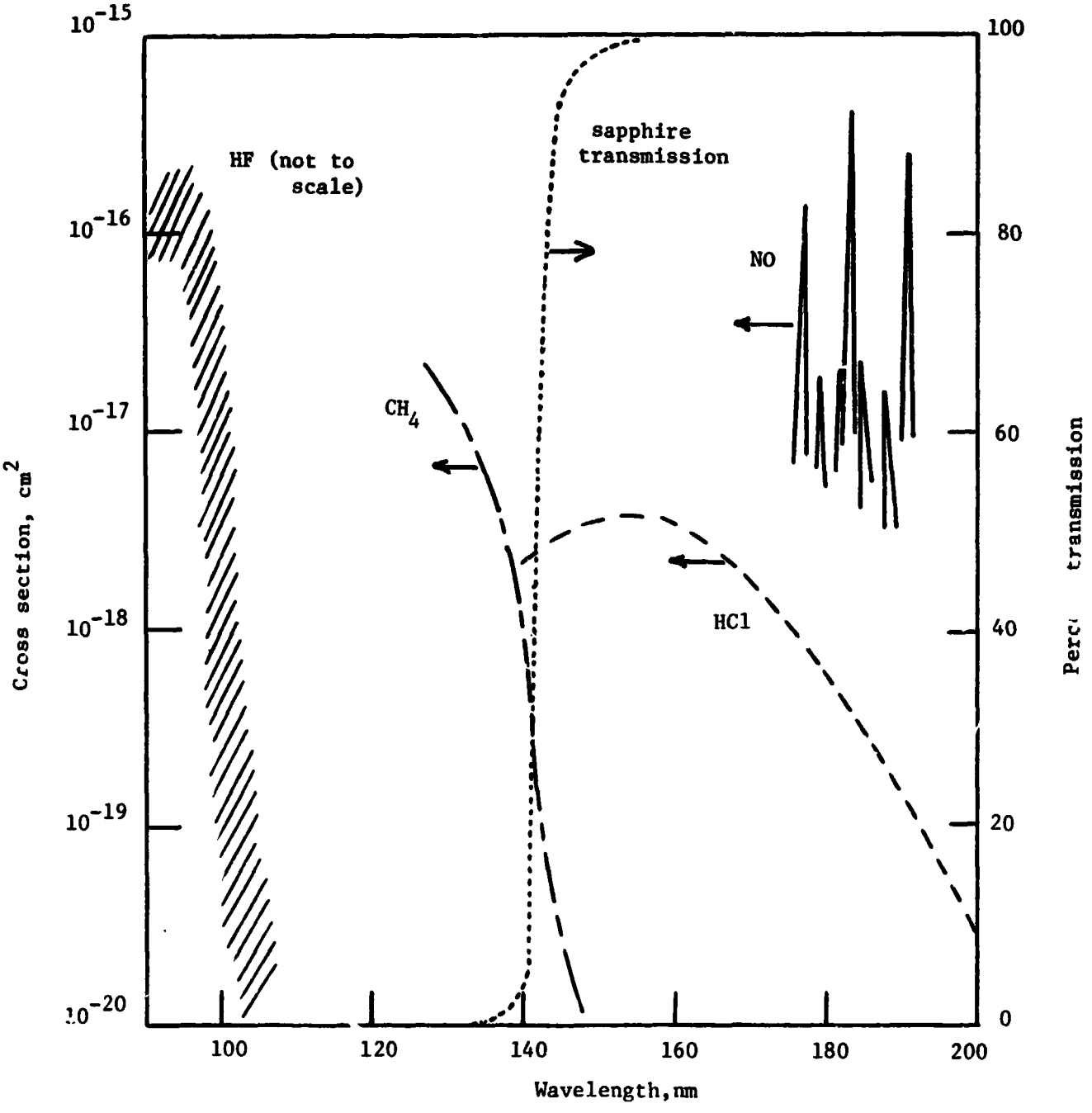

Figure 2.-Spectral cross sections of the four HALOE gases and transmission of sapphire.

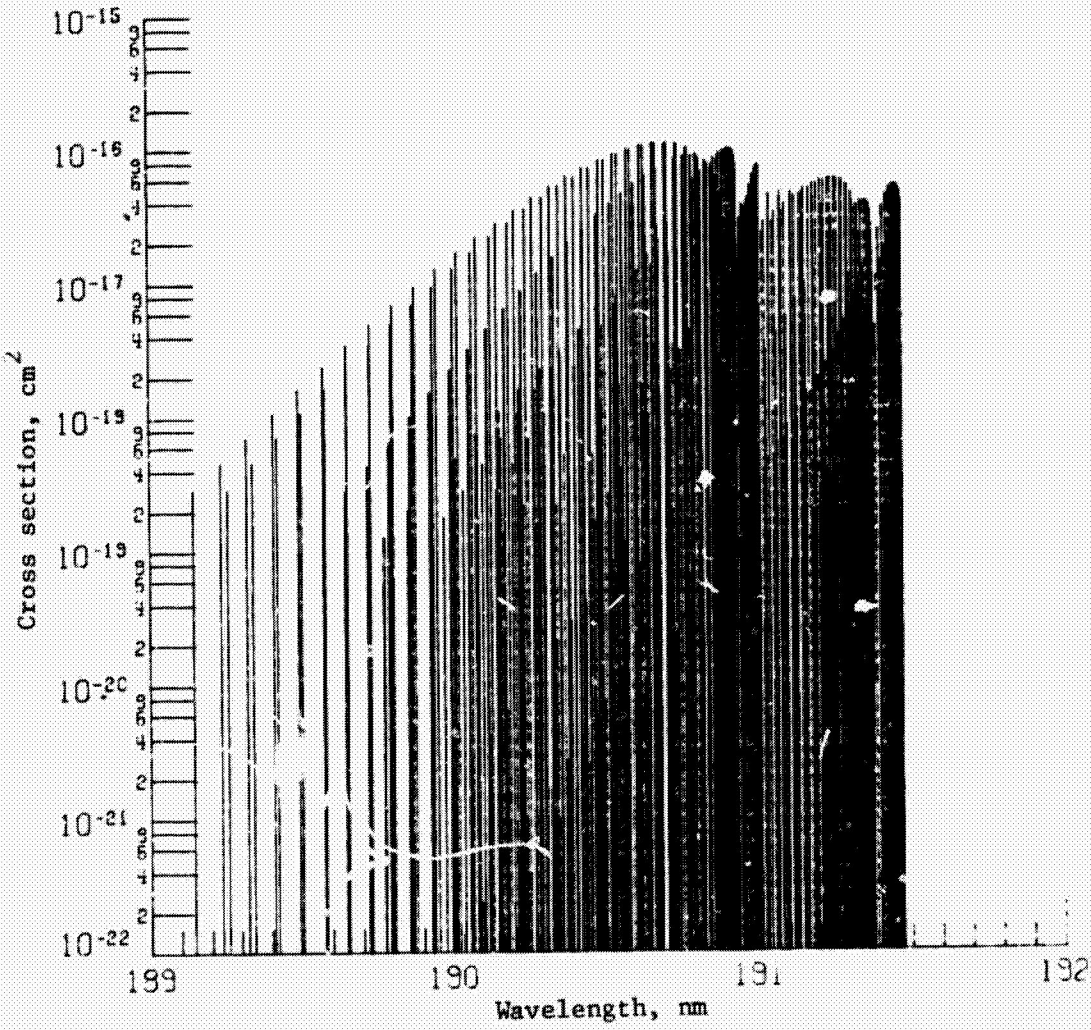

Figure 3(a)-Computer generated line spectrum of the 0-0 transition of the NO delta bands.

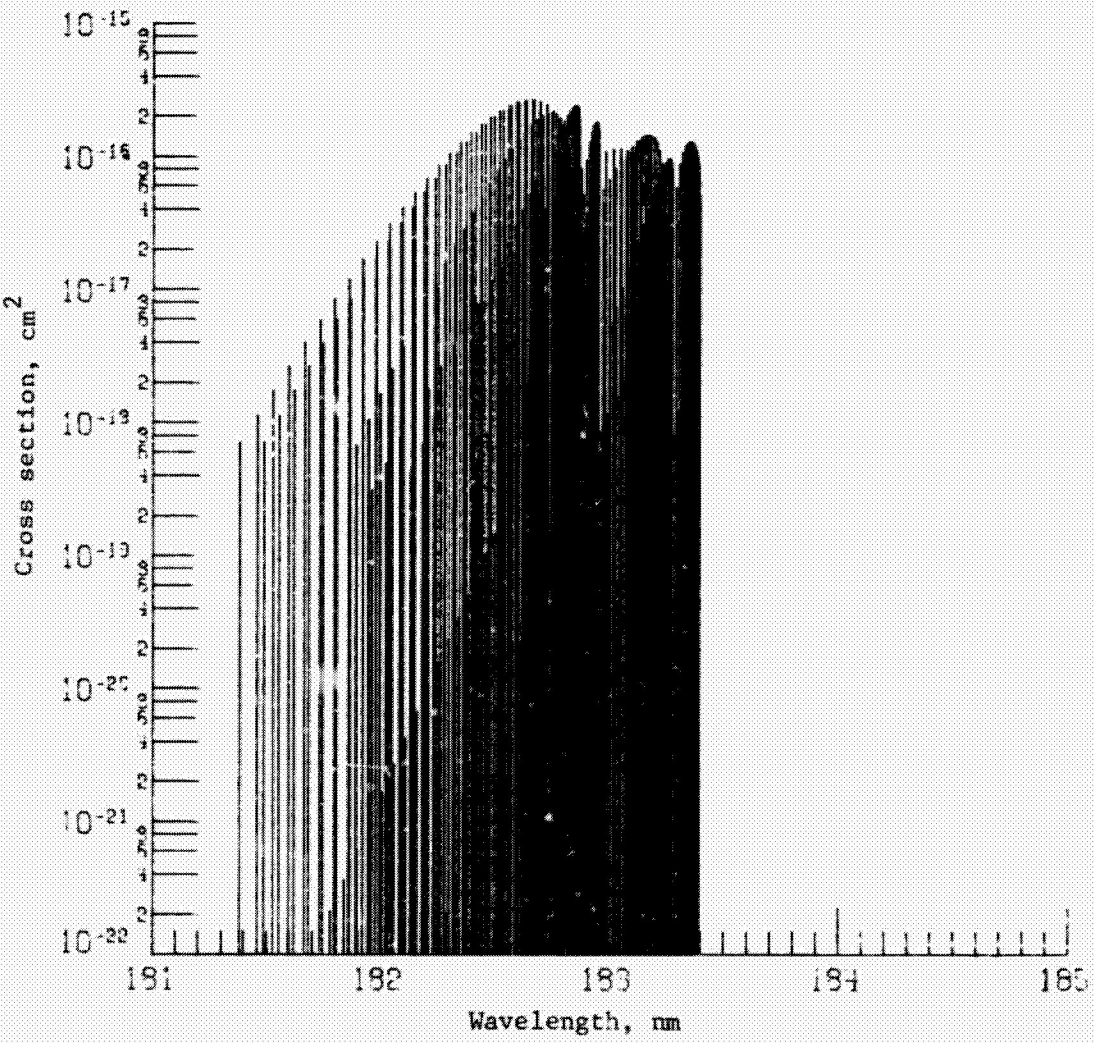

Figure 3(b)-Computer-generated line spectrum of the 1-0 transition of the NO delta bands.

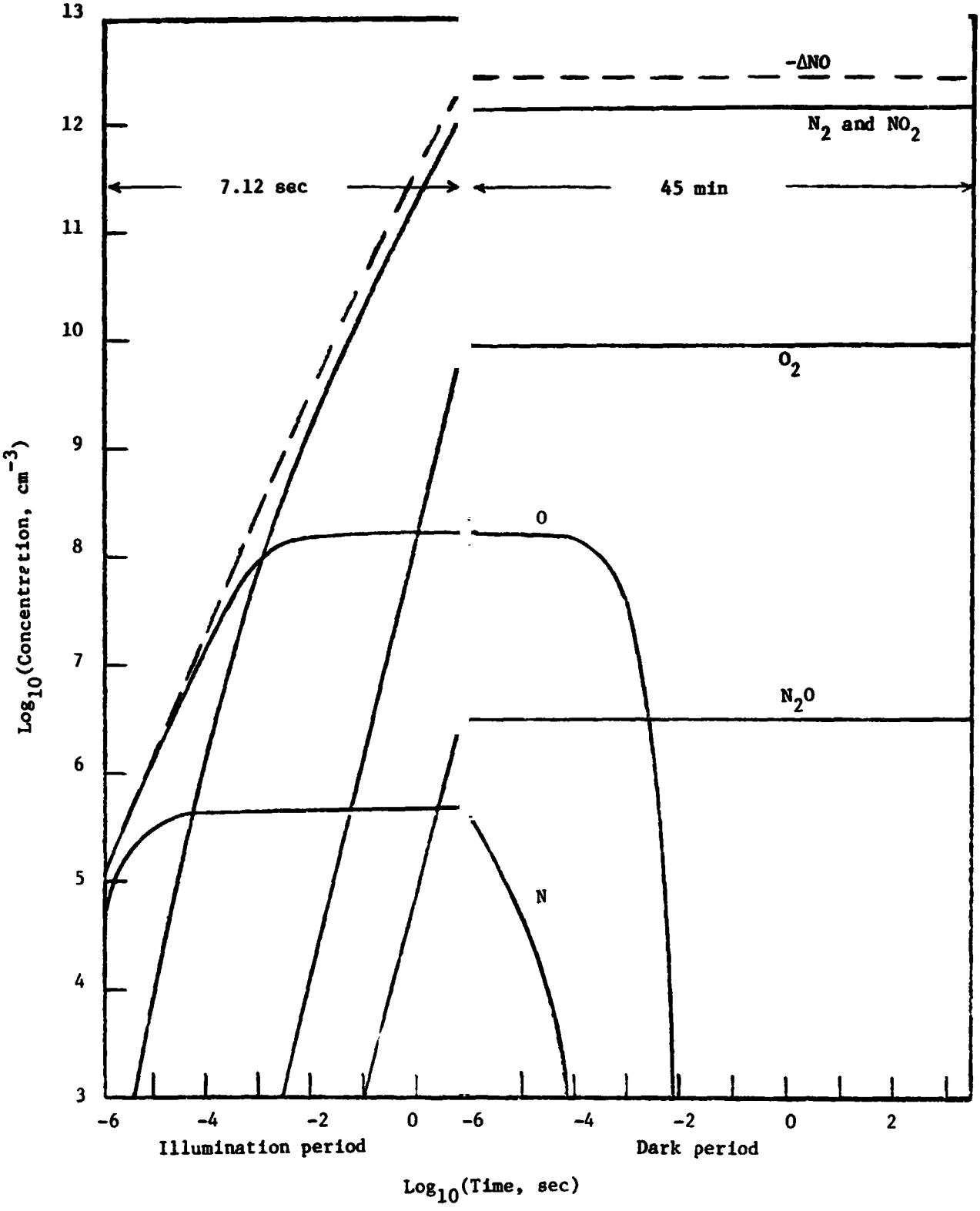

Figure 4.-Time-dependent chemistry calculation for initial exposure cycle and subsequent dark period for HALOE NO calibration cell.

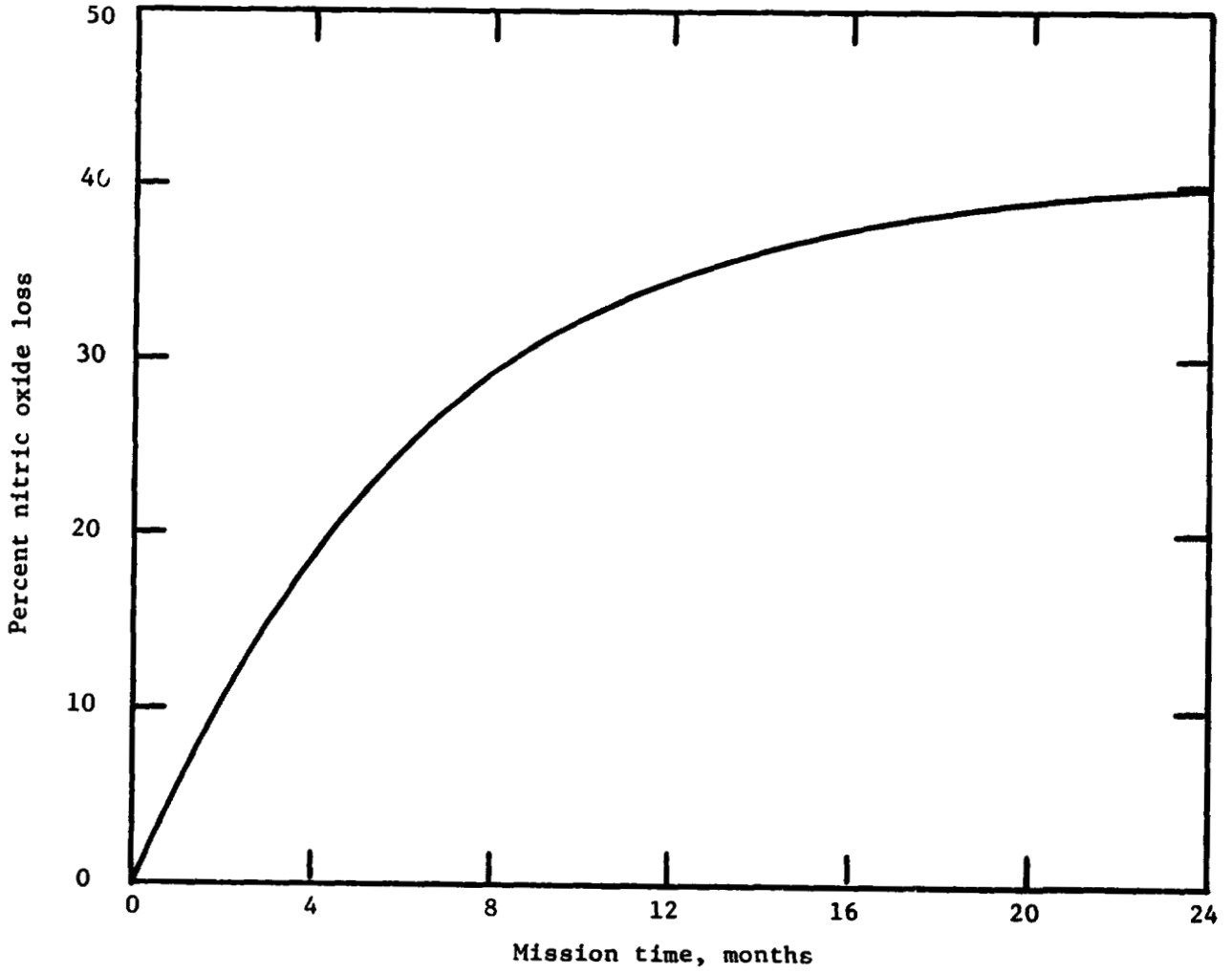

Figure 5.-Computed prediction of loss of NO due to solar flux in unprotected HALOE calibration cell.

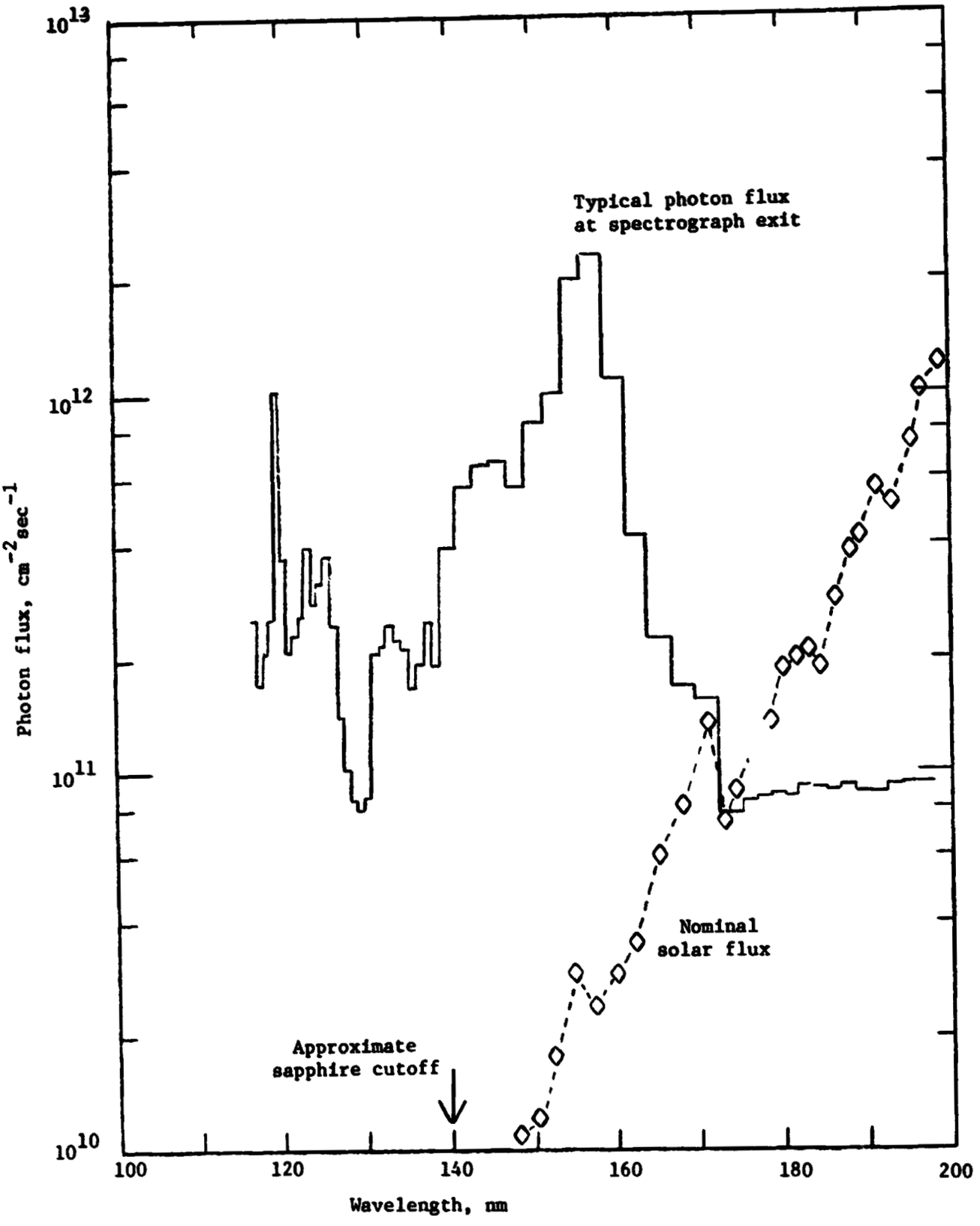

Figure 6.-Typical spectral solar flux and photon flux of the hydrogen discharge light source in the vacuum ultraviolet.

ORIGINAL PAGE
BLACK AND WHITE PHOTOGRAPH

Figure 1.—Photograph of vacuum spectrograph with hydrogen discharge lamp in foreground and detectors mounted on dual-beam attachment at exit aperture.

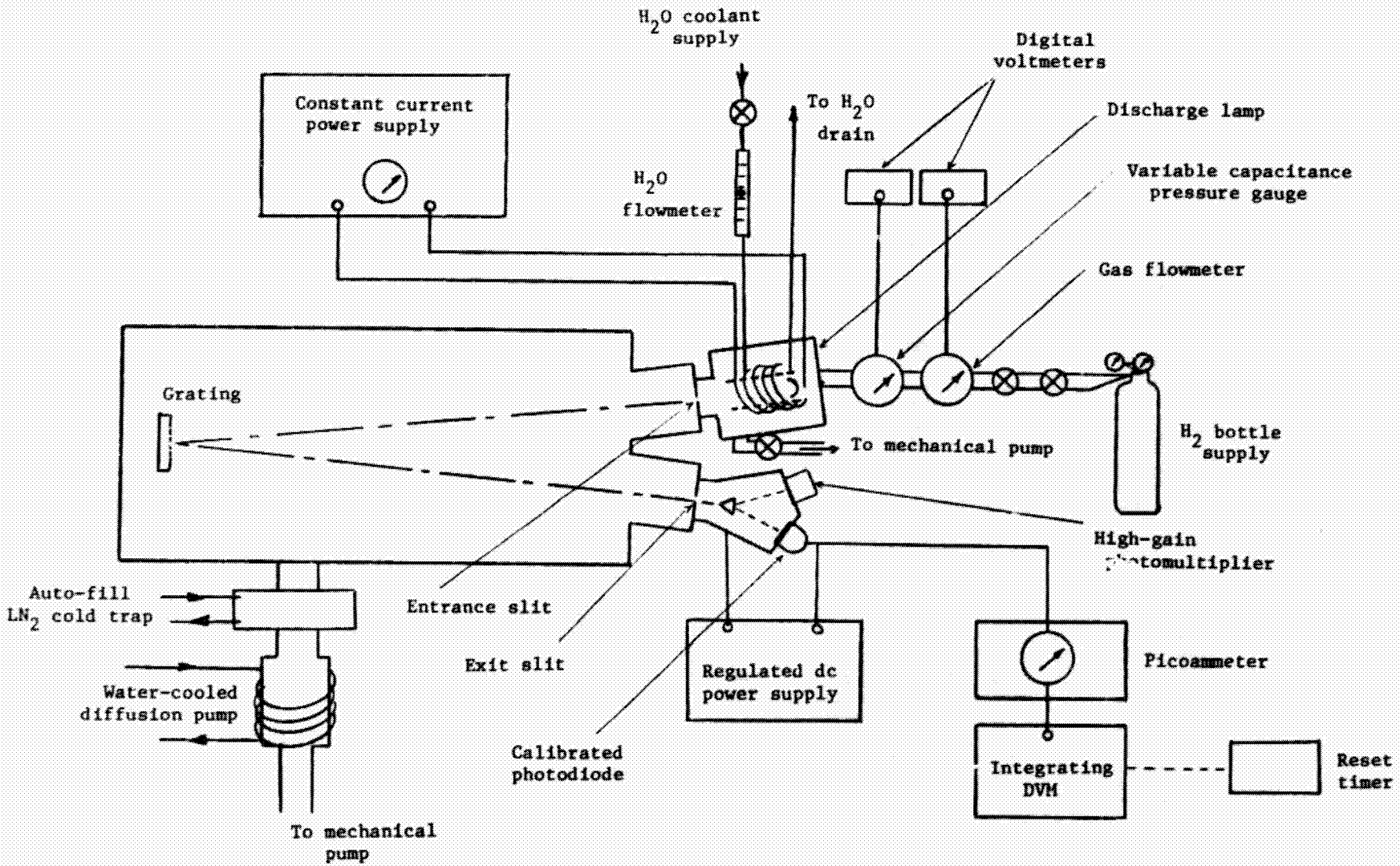

Figure 8.-Diagram of 1-meter spectrograph with hydrogen discharge lamp and peripheral equipment.

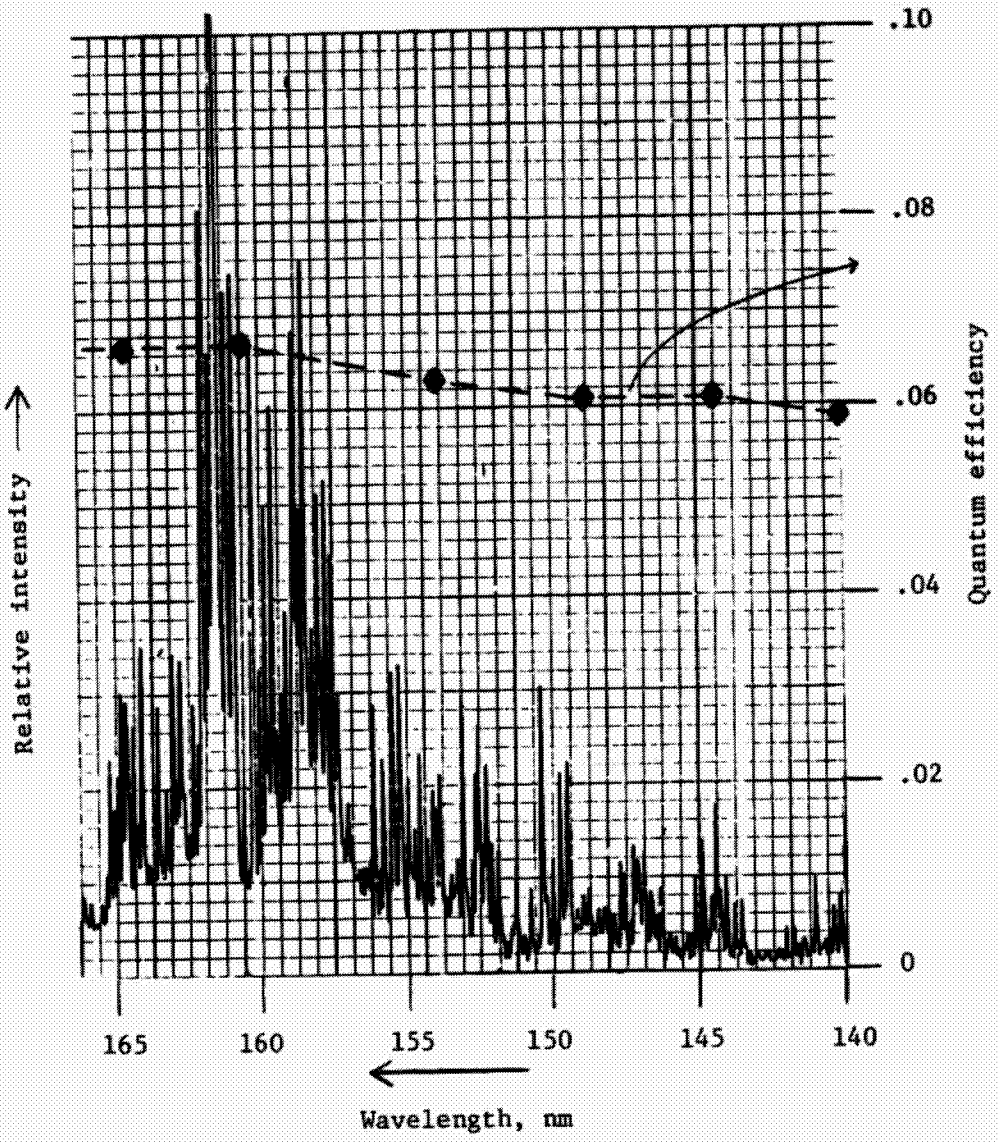

Figure 9.-Spectral scan of hydrogen lamp in the region of greatest intensity and measured quantum efficiency of photodiode calibrated at NBS.

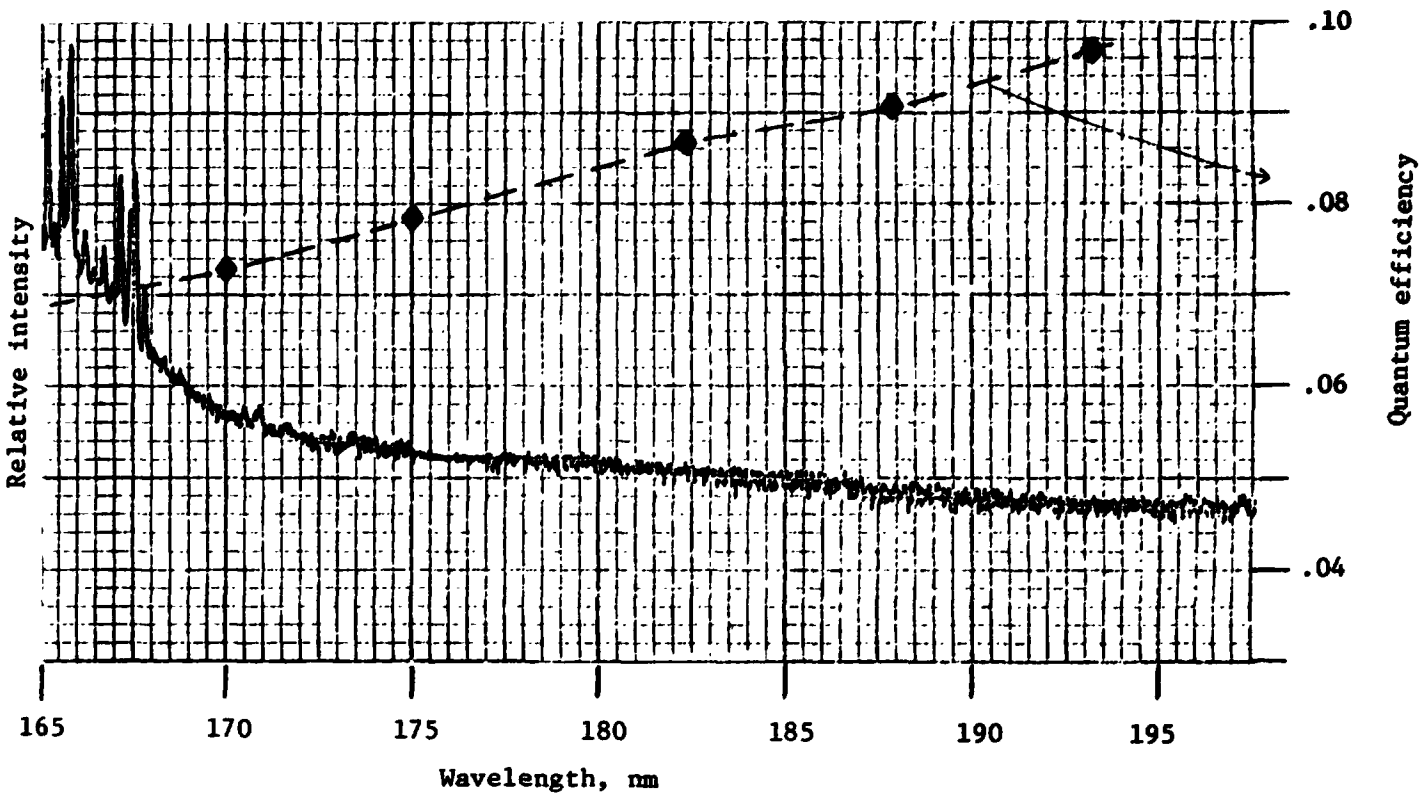

Figure 10.-Spectral scan of hydrogen lamp intensity in the continuum region and measured quantum efficiency of photodiode calibrated at NBS.

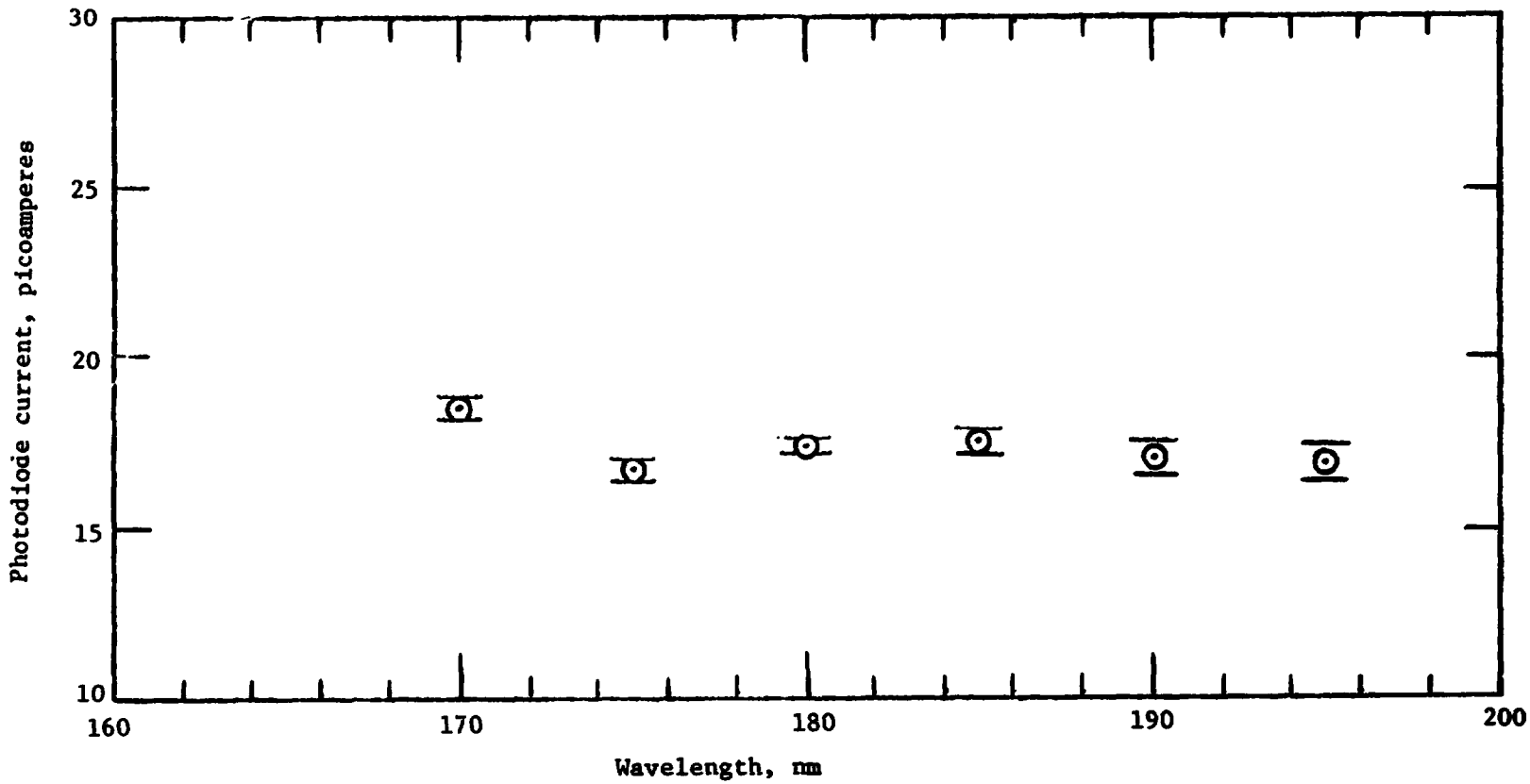

Figure 11.- Hydrogen lamp spectral intensity measurements in the continuum region. The range of values at each wavelength is indicated for eight measurement sets taken over a two-week period.

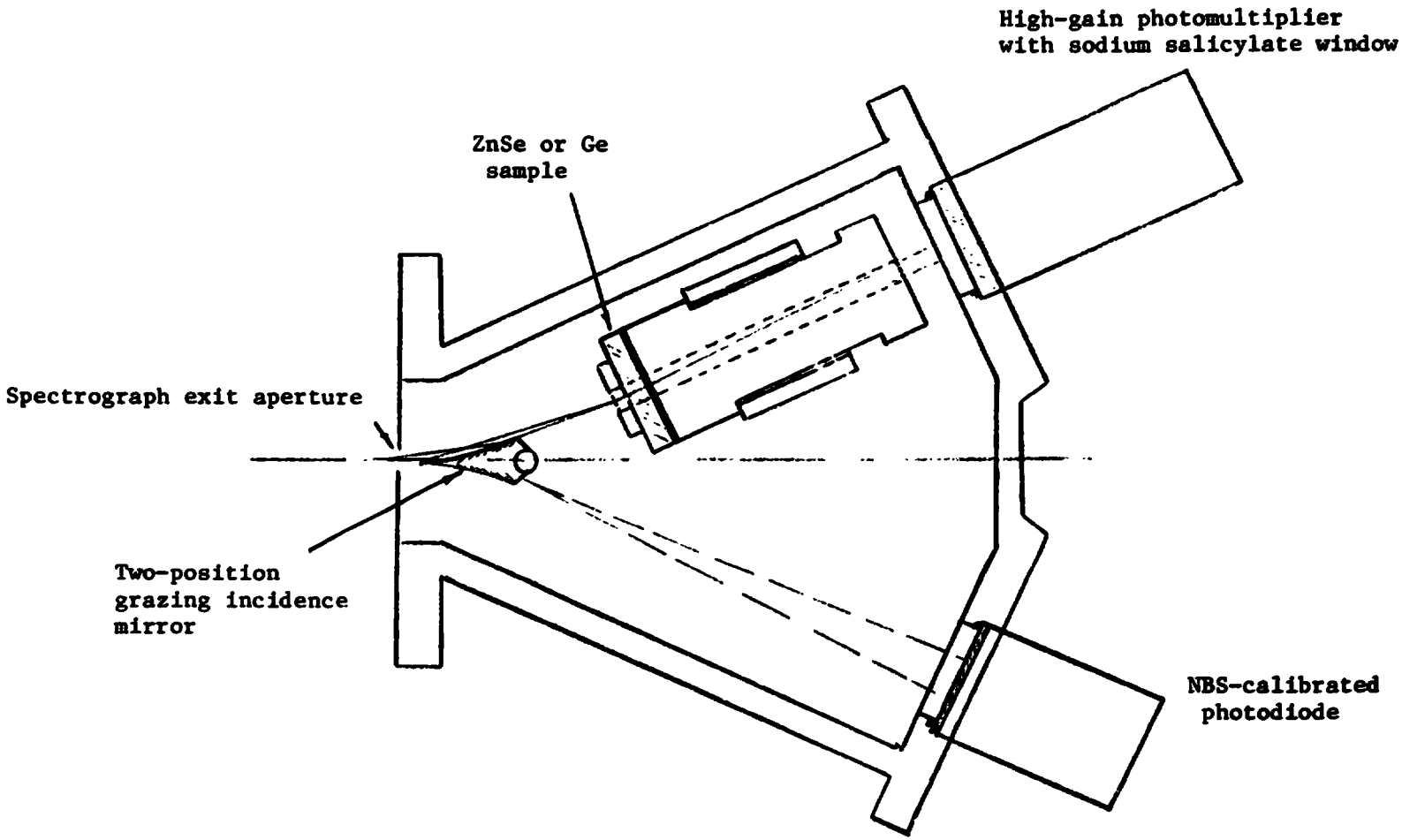

Figure 12.-Diagram of internal optical configuration of dual-beam attachment.

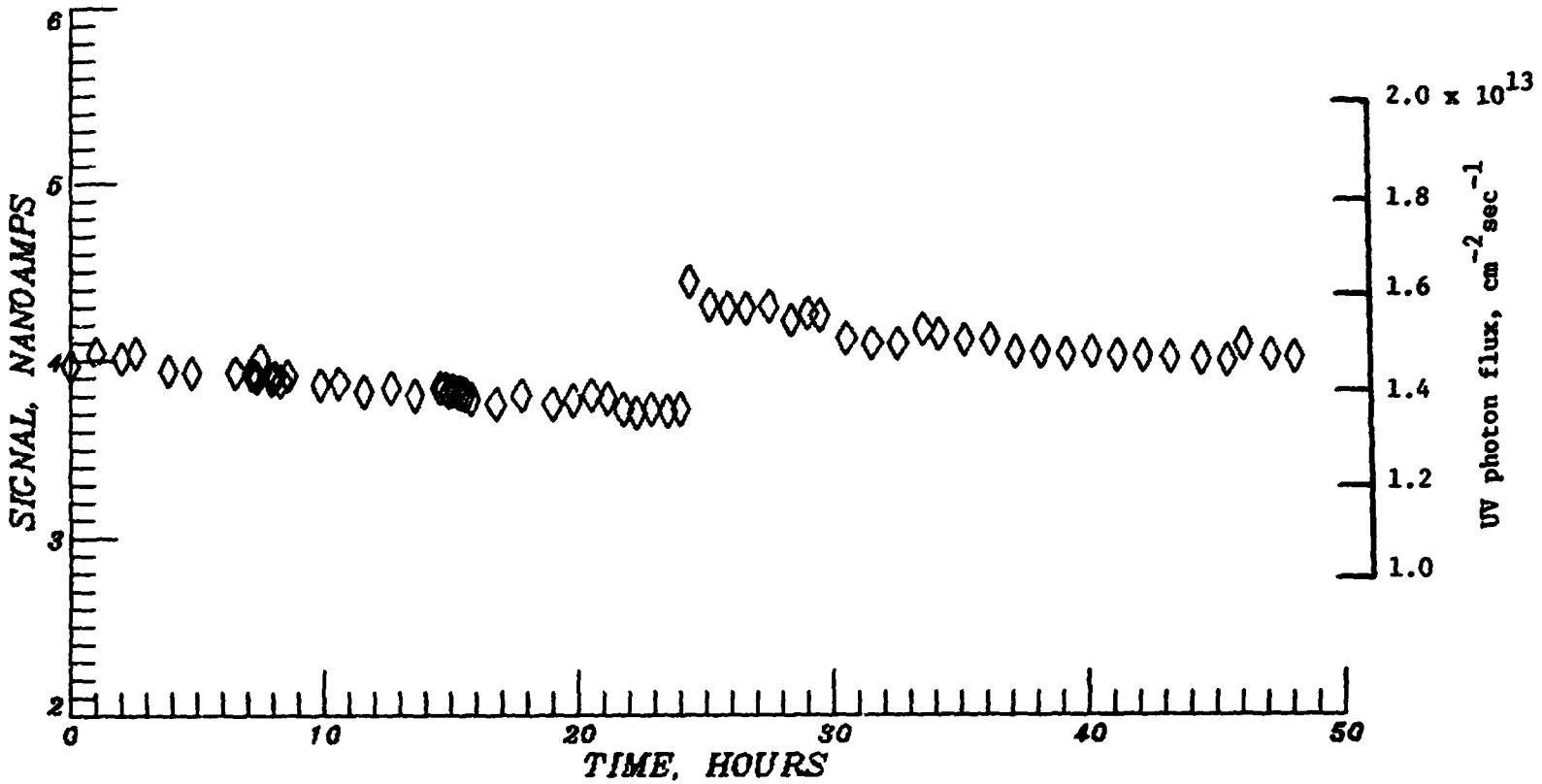

Figure 13(a)-Summary of exposure measurements for ZnSe sample. Photon flux scale is obtained by conversion described in text.
(The apparent discontinuity in lamp intensity at 24 hrs. occurred after an interruption in operation during which vacuum system repairs were made. Explicit reasons for this change are not known.)

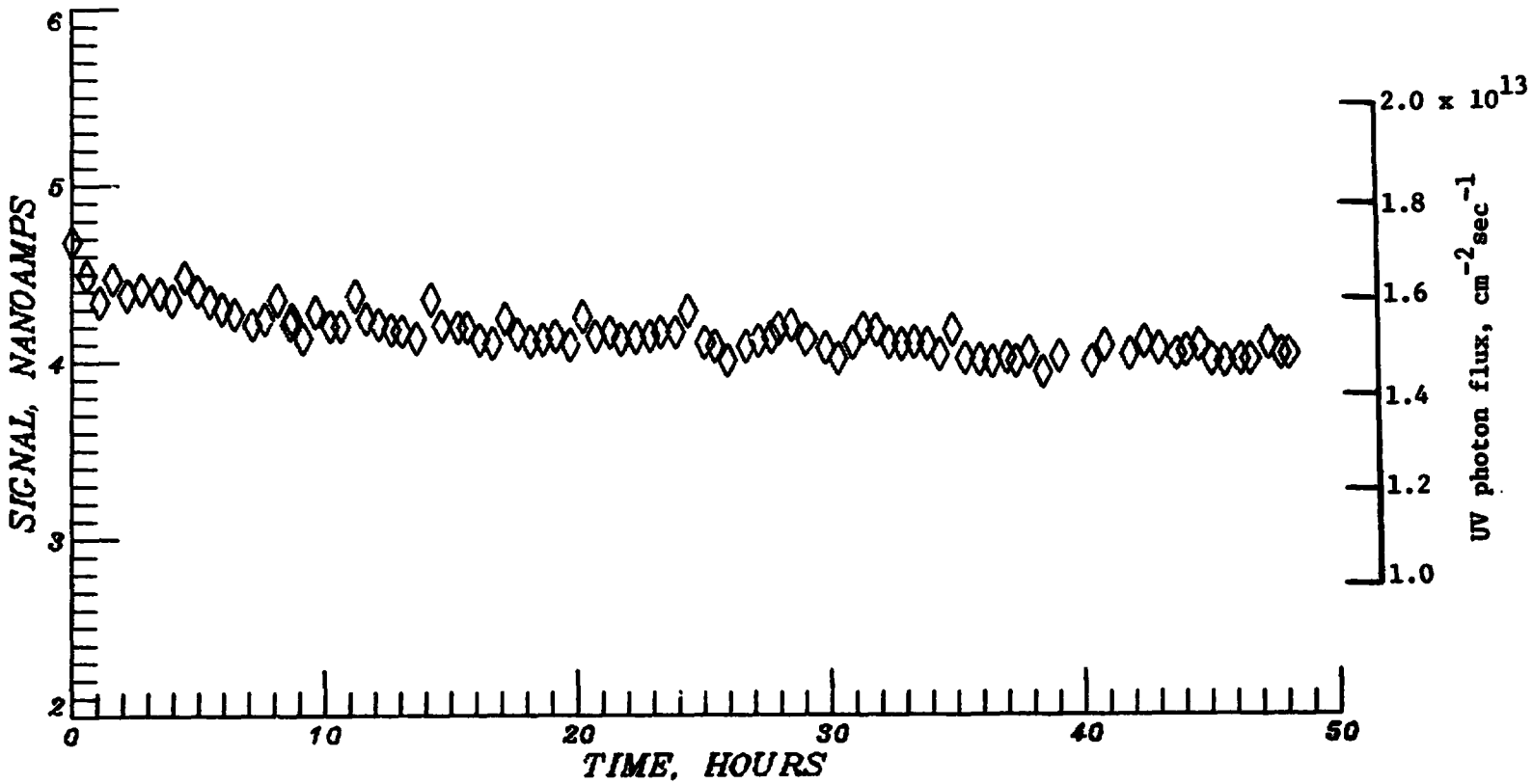

Figure 13(b)-Summary of exposure measurements for coated Ge sample.

ORIGINAL PAGE
BLACK AND WHITE PHOTOGRAPH

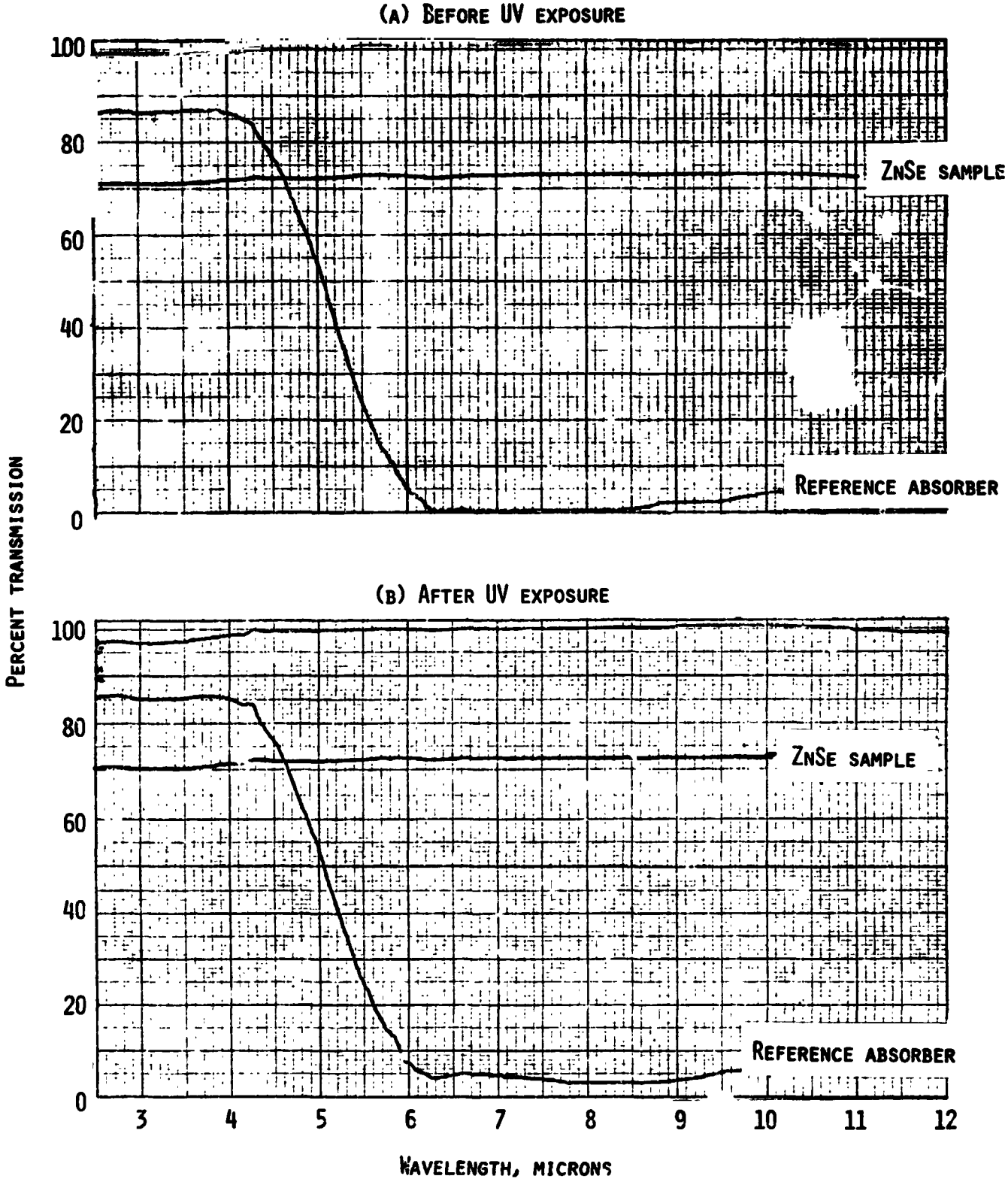

Figure 14.-Infrared transmission scans for zinc selenide test sample indicating no perceptible change in infrared characteristics.

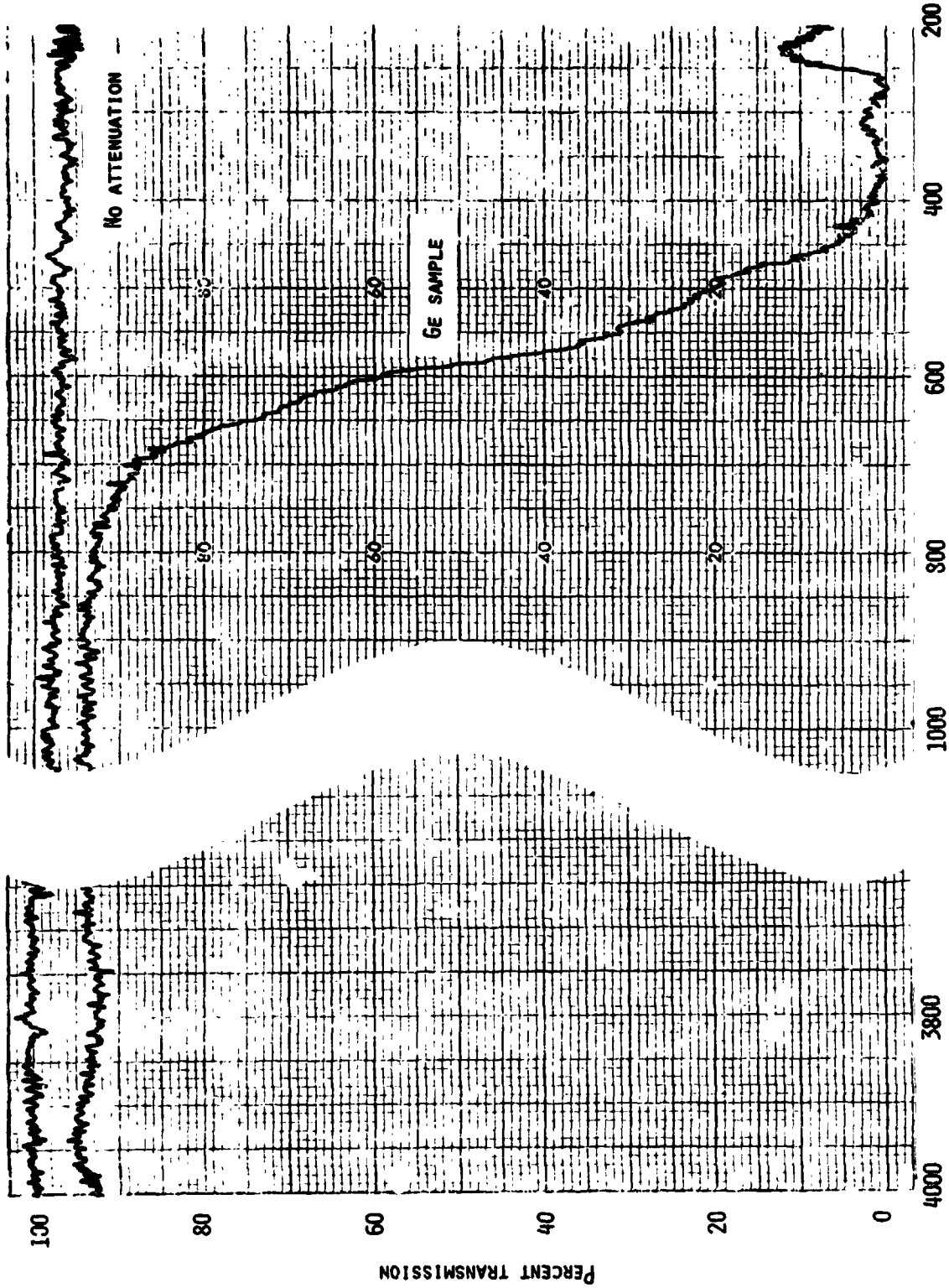

Figure 15(a)-Infrared transmission scan for coated germanium sample before UV exposure. (Transmission in omitted wavenumber range is essentially level.)

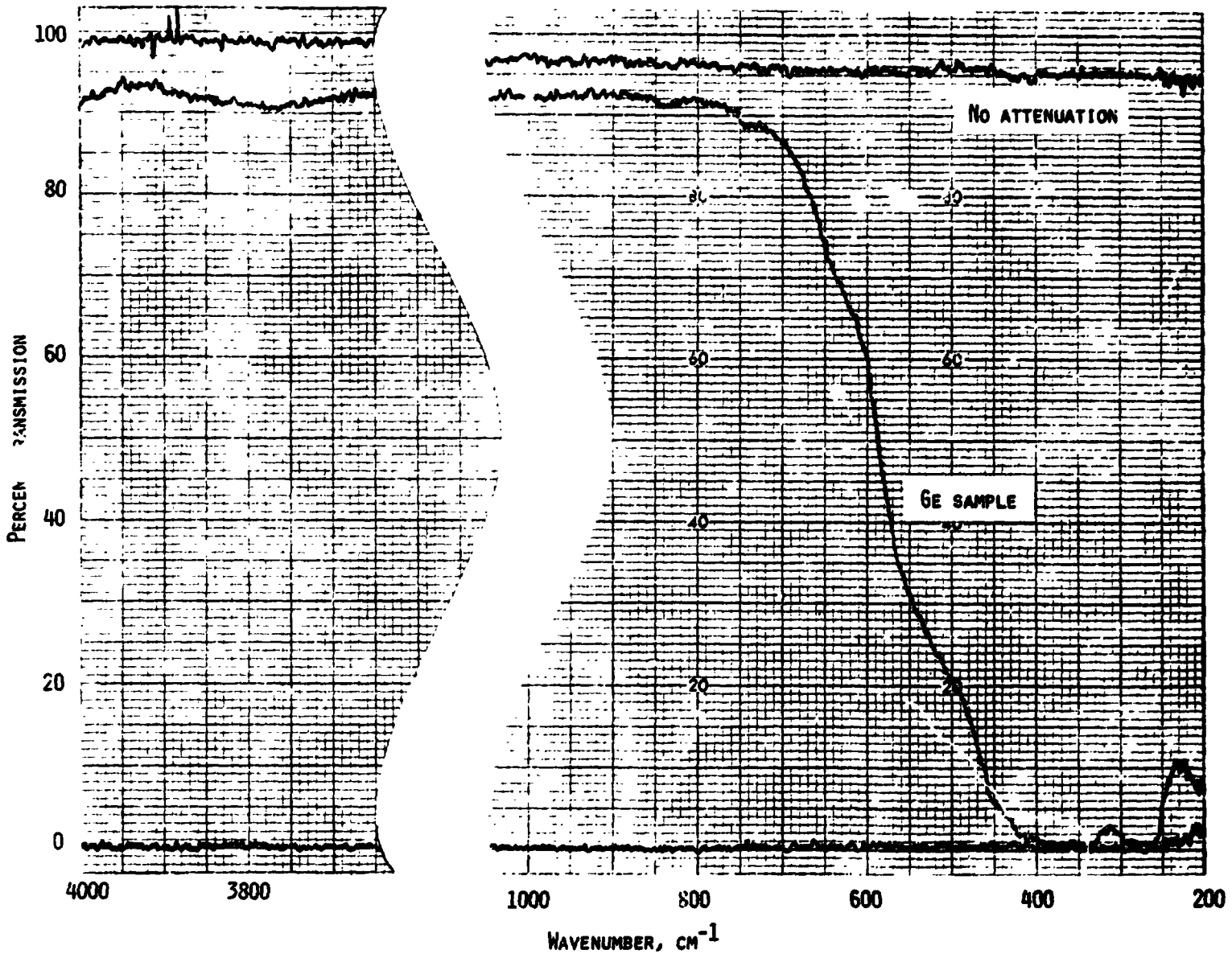

Figure 15(b)-Infrared transmission scan for coated germanium sample after UV exposure indicating no perceptible change in infrared characteristics. (Transmission in omitted wavenumber range is essentially level.)